JOURNAL OF COMPUTATIONAL PHYSICS 59, 108–119 (1985)

An Implicit Algorithm for Compressible Three-Dimensional Magnetohydrodynamic Calculations

A. Y. AYDEMIR AND D. C. BARNES

Institute for Fusion Studies, University of Texas, Austin, Texas 78712

Received February 7, 1984; revised May 1, 1984

An efficient algorithm for the solution of compressible magnetohydrodynamic equations in a three-dimensional geometry is presented. Compressional Alfvén waves are treated implicitly, thus greatly increasing the stable time step of the calculation and making it possible to study magnetohydrodynamic (MHD) phenomenon on resistive time scales.

1. INTRODUCTION

In recent years numerous algorithms have been developed to solve various forms of the magnetohydrodynamic (MHD) equations in three-dimensional geometries. One quite successful approach has made use of the reduced MHD equations [1, 2]. Early calculations along these lines have retained only the leading order terms in the aspect ratio expansions [3–6], while recently some tokamak calculations have included higher order corrections [7, 8]. Although these algorithms are quite efficient, they inherently have limited applicability, since a tokamak ordering is used in the derivation of the equations; i.e., $B_\theta/B_\zeta \sim O(\varepsilon)$, where B_θ and B_ζ are the poloidal and toroidal components of the magnetic field, and ε is the ratio of the minor to major radius of the torus.

A second approach with more general applications uses the primitive, non-reduced MHD equations. However, the compressional Alfvén waves, which are ordered out of the system in the low order reduced equations, cause severe time step restrictions in the direct application of the primitive equations. Explicit algorithms which follow phenomena occurring on this fast compressional time scale, even when they employ highly efficient spectral techniques [9], are not quite suitable for studying the nonlinear evolution of resistive MHD modes, which occurs on a much longer time scale. An implicit algorithm based on ADI technique was presented by Finan [10]; however, it uses a three-dimensional grid and is subject to the inefficiencies and inaccuracies of finite difference techniques in a three-dimensional geometry.

At the expense of ignoring some relevant physics, the problem associated with compressional waves can be overcome by assuming the fluid flow to be incompressible, which removes the fast Alfvén waves from the system. An algorithm that

0021-9991/85 $3.00

makes use of the incompressible MHD equations has been presented earlier [11, 12] and applied to the study of resistive kink modes in the Reversed Field Pinch (RFP) [13]. In these works, without the presence of the compressional waves, it has been possible to study the sustainment of the reversed field in the RFP on a resistive time scale.

The incompressibility assumption is not strictly valid, especially in an RFP, and needs to be justified a posteriori. For this purpose, we have developed an algorithm that solves the compressible MHD equations in a three-dimensional geometry [14]. So as not to be limited by the compressional time scale, however, those terms in the equations that drive the compressional waves are treated implicitly. The maximum stable time step in the resulting algorithm is determined by the shear Alfvén waves, as in the incompressible equations, and it is more than an order of magnitude larger than the time step of a corresponding explicit calculation. A somewhat similar algorithm for implicit treatment of compressional waves has been presented earlier by Jardin for two dimensional ideal MHD calculations [15].

The outline of the paper is as follows. In the next section the equations used in our compressible code (CTD) will be summarized. The implicit algorithm will be discussed in Section 3. In Section 4, comparisons will be made between implicit and explicit versions of the code, and some preliminary results from RFP calculations will be presented and compared with our earlier incompressible results. Section 5 will summarize the paper.

2. Equations

The compressible, nonlinear, resistive magnetohydrodynamic equations are written in the following form:

$$\frac{\partial \rho}{\partial t} + (\mathbf{u} \cdot \nabla)\, \rho = -\rho \nabla \cdot \mathbf{u}, \tag{1}$$

$$\rho \left[\frac{\partial \mathbf{u}}{\partial t} + (\mathbf{u} \cdot \nabla)\, \mathbf{u} \right] = \mathbf{J} \times \mathbf{B} - \nabla p + \nu \left[-\nabla \times \nabla \times \mathbf{u} + \frac{4}{3} \nabla (\nabla \cdot \mathbf{u}) \right], \tag{2}$$

$$\frac{\partial \mathbf{A}}{\partial t} = \mathbf{u} \times \mathbf{B} - \frac{1}{S} \mathbf{J}, \tag{3}$$

$$\frac{\partial p}{\partial t} + (\mathbf{u} \cdot \nabla)\, p = -\Gamma p \nabla \cdot \mathbf{u}, \tag{4}$$

$$\mathbf{B} = \nabla \times \mathbf{A}, \tag{5}$$

$$\mathbf{J} = \nabla \times \mathbf{B}. \tag{6}$$

The variables have their usual meanings. ρ is the mass density; $\mathbf{u}$, $\mathbf{B}$, and $\mathbf{E}$ are velocity, magnetic, and electric fields, respectively; and p is the kinetic pressure.

Instead of **B**, the vector potential **A** is advanced in time using a gauge in which the scalar potential vanishes. Γ is the ratio of the specific heats. S, the magnetic Reynolds number, is the ratio of the diffusion time $\tau_r = \mu_0 a^2/\eta$ to the Alfvén time $\tau_h = a/u_h$, where $u_h = B_0/(\mu_0 \rho_0)^{1/2}$, and ν is the coefficient of viscosity. The scale length a is the minor radius. B_0 and ρ_0 are, respectively, the characteristic field strength and mass density used in the normalizations. In the present version of the code, a uniform mass density ($\rho = 1$) is assumed, and Eq. (1) is dropped from the system.

3. Numerical Methods

Equations (2)–(6) are solved in a cylindrical geometry with periodic end boundary conditions. As in the incompressible algorithm ITD [12], the variables are expanded in Fourier series in the periodic coordinates θ and ζ. The angle ζ is related to the usual coordinate z through $\zeta = z/R_0$, where R_0 is the normalized major radius. Finite differences are used in the radial direction with a staggered mesh [12].

The quadratic nonlinearities in Eqs. (2)–(4) lead to convolution sums in the Fourier space which are treated either through direct summations, or using Fast Fourier Transforms (FFT) [16]. When FFTs are used, aliasing errors introduced by the discrete transforms quickly degrade the solution, especially in the higher harmonics. For long time study of MHD phenomena, we have found it necessary to remove these errors. This "dealiasing" is accomplished by embedding the quantities to be convoluted in approximately 50% longer arrays in each of the two transform directions [16]. Using the one-dimensional sum

$$w(m) = \sum_{m'} u(m')\, v(m - m'), \qquad -M < m,\ m' \leqslant M,$$

as an example, the dealiased FFT convolution proceeds as follows.

First, arrays $\hat{u}(m)$, $\hat{v}(m)$ are defined as

$$(\hat{u}(m), \hat{v}(m)) = (u(m), v(m)) \qquad \text{for} \quad -M < m \leqslant M,$$

$$(\hat{u}(m), \hat{v}(m)) = (0, 0) \qquad \text{for} \quad -\hat{M} < m \leqslant -M,\ M < m \leqslant \hat{M},$$

where $\hat{M}$ is determined by $M \leqslant 2\hat{M}/3$ using integer arithmetic. Then

$$w(m) = \mathrm{FFT}^{-1}(\mathrm{FFT}(\hat{u}) \times \mathrm{FFT}(\hat{v})) \qquad \text{for} \quad -M < m \leqslant M,$$

$$w(m) = 0 \qquad \text{otherwise.}$$

Note that since $\hat{M}$ needs to be in the form 2^p, where p is an integer, in calculations using FFT convolutions, first the mode numbers $\hat{M}$, $\hat{N}$ are chosen, from which the boundaries of the dealiased region in the Fourier space are determined using $M \leqslant 2\hat{M}/3$, $N \leqslant 2\hat{N}/3$.

Using Buneman's vectorized FFT subroutine VCFT [17], and performing two real transforms simultaneously, dealiased FFT convolutions with $\hat{M} = \hat{N} = 8$, and the corresponding direct summations with $M = N = 5$ require approximately equal amounts of time on the Cray-1. For larger number of modes, FFT convolutions are more efficient.

3.1. *Temporal Differencing*

As in the solution of incompressible equations [12], a first order predictor–corrector scheme is used to advance Eqs. (2)–(6) in time. In the predictor step, provisional values $\mathbf{u}^*$, $\mathbf{A}^*$, and p^* are calculated using the equations

$$\mathbf{u}^* = \mathbf{u}^n + \delta t[-(\mathbf{u}^n \cdot \nabla)\,\mathbf{u}^n + \mathbf{J}^n \times \mathbf{B}^n - \nabla p^n], \tag{7}$$

$$\mathbf{A}^* = \mathbf{A}^n + \delta t[\mathbf{u}^n \times \mathbf{B}^n], \tag{8}$$

$$p^* = p^n + \delta t[-(\mathbf{u}^n \cdot \nabla)\,p^n - \Gamma p^n \nabla \cdot \mathbf{u}^n], \tag{9}$$

$$\mathbf{B}^* = \nabla \times \mathbf{A}^*, \quad \mathbf{J}^* = \nabla \times \mathbf{B}^*. \tag{10}$$

Time-step splitting is used in the corrector step to separate the viscous and ohmic dissipation terms from the rest of the quantities:

$$\hat{\mathbf{u}}^{n+1} = \mathbf{u}^n + \delta t\left[-(\mathbf{u}^* \cdot \nabla)\,\mathbf{u}^* + \mathbf{J}^* \times \mathbf{B}^* + \nabla \frac{\mathbf{B}^{*2}}{2} - \nabla \hat{\Pi}^{n+1}\right], \tag{11}$$

$$\hat{\mathbf{A}}^{n+1} = \mathbf{A}^n + \delta t[\hat{\mathbf{u}}^{n+1} \times \mathbf{B}^*], \tag{12}$$

$$\hat{p}^{n+1} = p^n + \delta t[-(\mathbf{u}^* \cdot \nabla)\,p^* - \Gamma p^* \nabla \cdot \hat{\mathbf{u}}^{n+1}], \tag{13}$$

$$\hat{\mathbf{B}}^{n+1} = \nabla \times \hat{\mathbf{A}}^{n+1}, \tag{14}$$

$$\Pi = p + \frac{\mathbf{B}^2}{2}, \tag{15}$$

$$\mathbf{u}^{n+1} = \hat{\mathbf{u}}^{n+1} + \delta t v\left[-\nabla \times \nabla \times \mathbf{u}^{n+1} + \frac{4}{3}\nabla(\nabla \cdot \mathbf{u}^{n+1})\right], \tag{16}$$

$$\mathbf{A}^{n+1} = \hat{\mathbf{A}}^{n+1} - \delta t \frac{1}{S} \nabla \times \nabla \times \mathbf{A}^{n+1}, \tag{17}$$

$$p^{n+1} = \hat{p}^{n+1}. \tag{18}$$

Note that in Eqs. (11)–(13), only those terms that drive the compressional waves are treated implicitly, which, as discussed in the Appendix, is necessary to avoid the time-step constraint set by the compressional Alfvén waves.

An obvious difficulty at this point is that Eqs. (11)–(15) cannot be solved easily, for the solution would require inversion of a system of the form

$$\mathbf{A} \cdot \hat{\mathbf{U}}^{n+1} = \mathbf{F},$$

where $\hat{\mathbf{U}}^{n+1} = (\hat{\mathbf{u}}^{n+1}, \hat{\mathbf{A}}^{n+1}, \hat{p}^{n+1})^t$. The matrix $\mathbf{A}$ will in general have rank $(7I(\mathrm{MN}))$, where I is the number of radial grid points, and (MN) is the total number of Fourier modes. Inversion of such large matrices at each time step is difficult and undesirable. Thus, the most important part of the implicit algorithm employed in CTD involves the solution of the equations in the corrector step in an efficient manner. This algorithm is discussed in the next section.

3.2. *Solution of the Corrector Equations*

To solve the corrector equations efficiently, the quantities defined in Eqs. (11)–(13) are first expanded about the known predictor quantities:

$$\hat{\mathbf{u}}^{n+1} = \mathbf{u}^* + \delta\mathbf{u}^{n+1}, \tag{19}$$

$$\hat{\mathbf{A}}^{n+1} = \mathbf{A}^* + \delta\mathbf{A}^{n+1}, \tag{20}$$

$$\hat{p}^{n+1} = p^* + \delta p^{n+1}. \tag{21}$$

Now if Eqs. (19)–(21) are substituted into Eqs. (11)–(13), we get

$$\delta\mathbf{u}^{n+1} = \Delta\mathbf{u} - \delta t\, \nabla\, \delta\Pi^{n+1}, \tag{22}$$

$$\delta\mathbf{A}^{n+1} = \Delta\mathbf{A} + \delta t\, \delta\mathbf{u}^{n+1} \times \mathbf{B}^*, \tag{23}$$

$$\delta p^{n+1} = \Delta p - \delta t\, \Gamma p^* \nabla \cdot \delta\mathbf{u}^{n+1}, \tag{24}$$

where $\Delta\mathbf{u}$, $\Delta\mathbf{A}$, and Δp are the known errors in satisfying Eqs. (11)–(13) with the predictor quantities. Specifically,

$$\Delta\mathbf{u} = \mathbf{u}^n - \mathbf{u}^* + \delta t[-(\mathbf{u}^* \cdot \nabla)\,\mathbf{u}^* + \mathbf{J}^* \times \mathbf{B}^* - \nabla p^*], \tag{25}$$

$$\Delta\mathbf{A} = \mathbf{A}^n - \mathbf{A}^* + \delta t[\mathbf{u}^* \times \mathbf{B}^*], \tag{26}$$

$$\Delta p = p^n - p^* + \delta t[-(\mathbf{u}^* \cdot \nabla)\, p^* - \Gamma p^* \nabla \cdot \mathbf{u}^*]. \tag{27}$$

Note that an explicit algorithm is obtained by letting

$$\hat{\mathbf{u}}^{n+1}_{\exp} = \Delta\mathbf{u} + \mathbf{u}^*, \tag{28}$$

$$\hat{\mathbf{A}}^{n+1}_{\exp} = \Delta\mathbf{A} + \mathbf{A}^*, \tag{29}$$

$$\hat{p}^{n+1}_{\exp} = \Delta p + p^*. \tag{30}$$

Thus, $\Delta\mathbf{u}$, $\Delta\mathbf{A}$, and Δp are the explicit corrections, whereas $\delta\mathbf{u}^{n+1}$, $\delta\mathbf{A}^{n+1}$, and δp^{n+1} are the implicit corrections to be added to the corrector values to obtain the corresponding explicit, and implicit values, respectively, at the new time step.

The $\delta\Pi^{n+1}$ term in Eq. (22) is the difference between the total pressure at time $n+1$ and the total pressure computed from the predictor quantities. That is, Eqs. (22)–(24) are exactly equivalent to Eqs. (11)–(13) provided that

$$\delta\Pi^{n+1} = \left(p^{n+1} + \frac{(\mathbf{B}^{n+1})^2}{2}\right) - \left(p^* + \frac{\mathbf{B}^{*2}}{2}\right). \tag{31}$$

Since Eq. (31) contains $\mathbf{B}^{n+1}$ (and therefore $\delta\mathbf{A}^{n+1}$) quadratically, Eqs. (22)–(24) are nonlinear. At this point, the corrector system is linearized by redefining $\delta\Pi^{n+1}$ to be linear in $\delta\mathbf{B}^{n+1} = \hat{\mathbf{B}}^{n+1} - \mathbf{B}^* = \nabla \times \delta\mathbf{A}^{n+1}$. Thus, Eq. (31) is replaced by

$$\delta\Pi^{n+1} = \delta p^{n+1} + \mathbf{B}^* \cdot \delta\mathbf{B}^{n+1}, \tag{31'}$$

where $\delta p^{n+1} = p^{n+1} - p^*$.

From Eqs. (22)–(24) and (31′) follows a linear equation for the correction $\delta\Pi^{n+1}$,

$$\begin{aligned}\delta\Pi^{n+1} - \delta t^2[\Gamma p^* \nabla^2 \delta\Pi^{n+1} - \mathbf{B}^* \cdot \nabla \times \nabla\, \delta\Pi^{n+1} \times \mathbf{B}^*] \\ = -\delta t\, \Gamma p^* \nabla \cdot \Delta\mathbf{u} + \delta t\, \mathbf{B}^* \cdot \nabla \times \Delta\mathbf{u} \times \mathbf{B}^* + \mathbf{B}^* \cdot \Delta\mathbf{B} + \Delta p,\end{aligned} \tag{32}$$

where $\Delta\mathbf{B} = \nabla \times \Delta\mathbf{A}$.

While (32) is a linear equation for $\delta\Pi^{n+1}$, the left-hand side contains non-constant coefficients. Thus, all Fourier modes will be coupled, unless p^* and $\mathbf{B}^*$ depend only on radius. Although this is not generally the case, it has been determined empirically that stability is maintained for large time steps if only those terms resulting from θ and ζ independent components of p^* and $\mathbf{B}^*$ are retained in Eq. (32). Considering the order of those terms omitted, and the time-step constraint imposed by the shear Alfvén waves, this observation is equivalent to the mixing length argument that the deviation of a field line from the mean field position never exceeds the perpendicular scale length of the perturbation. Thus, the actual corrector equation to be solved is obtained by replacing p^* and $\mathbf{B}^*$ by their mean (radius dependent) values:

$$\begin{aligned}\delta\Pi^{n+1} - \delta t^2[\Gamma p_0^* \nabla^2 \delta\Pi^{n+1} - \mathbf{B}_0^* \cdot \nabla \times \nabla\, \delta\Pi^{n+1} \times \mathbf{B}_0^*] \\ = -\delta t\, \Gamma p_0^* \nabla \cdot \Delta\mathbf{u} + \delta t\, \mathbf{B}_0^* \cdot \nabla \times \Delta\mathbf{u} \times \mathbf{B}_0^* + \mathbf{B}_0^* \cdot \Delta\mathbf{B} + \Delta p.\end{aligned} \tag{32'}$$

To be consistent with Eq. (32′), the corrector equations (23), (24), and (31′) are also modified by replacing p^* and $\mathbf{B}^*$ by their mean values:

$$\delta\mathbf{A}^{n+1} = \Delta\mathbf{A} + \delta t\, \delta\mathbf{u}^{n+1} \times \mathbf{B}_0^*, \tag{23'}$$

$$\delta p^{n+1} = \Delta p - \delta t\, \Gamma p_0^* \nabla \cdot \delta\mathbf{u}^{n+1}. \tag{24'}$$

$$\delta\Pi^{n+1} = \delta p^{n+1} + \mathbf{B}_0^* \cdot \delta\mathbf{B}^{n+1}. \tag{31''}$$

The Fourier transform of Eq. (32′) is tridiagonal in radius for each (m, n) and is thus easily inverted. With $\delta\Pi^{n+1}$ determined, the remaining corrections are obtained using Eqs. (22), (23′), (24′), which are in turn substituted into Eqs. (19)–(21) to obtain $\hat{\mathbf{u}}^{n+1}$, $\hat{\mathbf{A}}^{n+1}$, and $\hat{p}^{n+1}$.

Finally in Eqs. (16), (17), implicit diffusion terms are added to complete the corrector step. These equations lead to block tridiagonal systems for $\mathbf{u}(r; mn)$ and $\mathbf{A}(r; mn)$, which are inverted using standard techniques [18].

4. Results

In this section, we will make specific comparisons between implicit and explicit versions of the code and present some preliminary results from RFP calculations, comparing them to our earlier incompressible results.

4.1. *Explicit versus Implicit Calculations*

An RFP calculation in which the nonlinear interaction of 58 Fourier modes on a radial grid with 64 points is performed using both the implicit and explicit versions of the code. The differences between the two calculations are summarized below:

(a) The average time step for the explicit calculation is 2.48×10^{-3}, whereas for the implicit one it is 5.13×10^{-2}. If the calculations are continued, this difference increases further, since $\langle \delta t \rangle_{\text{imp}} \simeq 0.1$ after the saturation of the dominant modes. Histories of $\langle \delta t \rangle = t/N_{\text{cyc}}$, where N_{cyc} is the number of cycles needed to reach time t, are shown in Figs. 1 and 2 for the implicit and explicit calculations, respectively. Note that $\langle \delta t \rangle_{imp}$ is comparable to the average time step we observe in our incompressible calculations.

(b) The implicit algorithm described above involves very little additional work compared to the corresponding explicit algorithm of Eqs. (28)–(30), since no convolutions are needed to obtain the implicit corrections. The work required for the solution of the elliptic equation (32′) for $\delta \Pi^{n+1}$ is insignificant compared to the work in performing the convolution sums resulting from the nonlinear terms in Eqs. (7)–(9), (25)–(27). Time spent (on a Cray-1) per mode, per mesh point, per time step for the explicit RFP calculation is 2.08×10^{-4} sec. For the implicit calculation this value is 2.16×10^{-4} sec. Thus, with only a slight increase in the work performed, the time step is increased by a factor of 20.

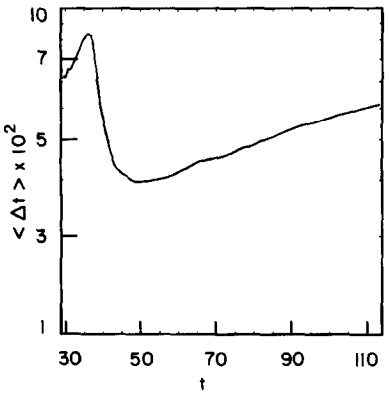

FIG. 1. Average time step $\langle \Delta t \rangle$ for the implicit calculation.

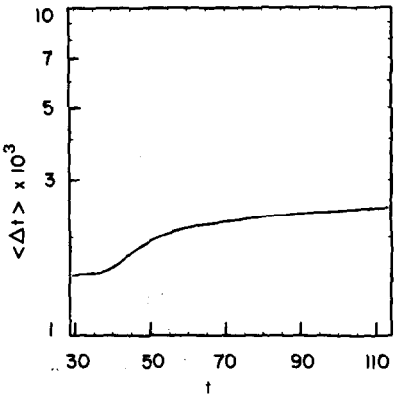

FIG. 2. Average time step for the explicit calculation.

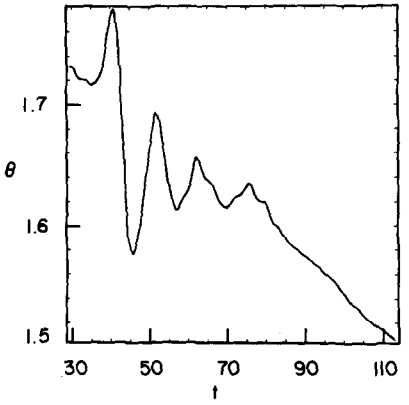

FIG. 3. Time history of the pinch parameter for the implicit calculation.

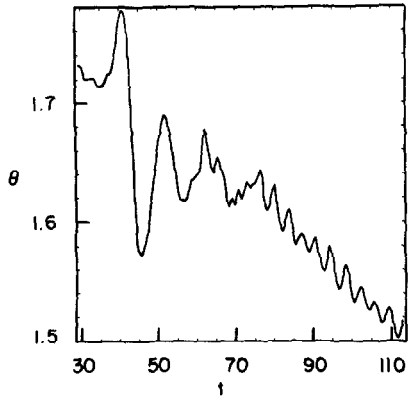

FIG. 4. Time history of the pinch parameter for the explicit calculation.

(c) Histories of the pinch parameter $\Theta = \langle B_\theta \rangle_{\text{wall}} / \langle B_\zeta \rangle_{\text{volume}}$ for the two calculations are shown in Figs. 3 and 4. The explicit calculation exhibits compressional oscillations, which are damped in the implicit one.

In the next section, comparisons between compressible and incompressible calculations are made.

4.2. *Compressible versus Incompressible Calculations*

Self-reversal of the toroidal field in an RFP, and the dynamo mechanism that sustains the reversal are studied using the implicit compressible code CTD, and the results are compared to our earlier incompressible calculations [13]. For this purpose, the implicit calculations of the previous section are continued with the boundary condition $\Theta_{\min} = 1.5$, i.e., the current is allowed to decay until the pinch parameter decreases to $\Theta_{\min}$, at which point a toroidal electric field is applied at the boundary preventing further decay of the current.

The dominant unstable modes of the initial zero-β equilibrium, $(m, n) = (1, 2)$, and $(m, n) = (1, 3)$, have growth rates that are larger by more than a factor of two in the compressible case. The saturation amplitudes of the modes are also larger (Fig. 5), which leads to a deeper initial reversal, as seen in the history plot of the reversal ratio $F = \langle B_\zeta \rangle_{\text{wall}} / \langle B_\zeta \rangle_{\text{volume}}$. These should be compared to the incompressible results in Fig. 6. A striking difference between these two cases is the lack of a true steady state in the compressible calculation, whereas the incompressible case exhibits a steady sustained reversal for $t > 450$. However, the results are qualitatively similar in that the compressible calculation also exhibits a sustained reversal, albeit with some fluctuations. Finally, it should be noted that the average time step for the implicit compressible run increases to 9.46×10^{-2} at the end of the calculation, with a gain of 38 over the corresponding explicit run.

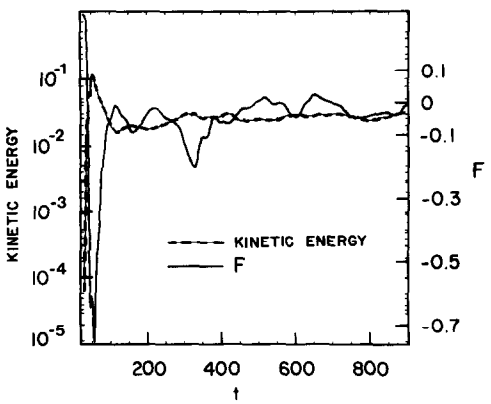

FIG. 5. Time history of the kinetic energy and the reversal ratio F for the implicit compressible calculation.

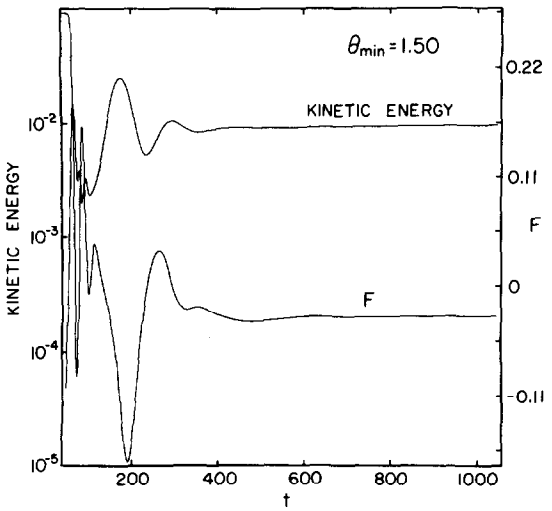

FIG. 6. Time history of the kinetic energy and the reversal ratio for the incompressible calculation.

5. SUMMARY

An efficient algorithm for the solution of compressible magnetohydrodynamic equations in a three-dimensional geometry has been developed. The compressional Alfvén waves, which ordinarily lead to a severe time-step restriction rendering meaningful calculations with these equations uneconomical, are treated implicitly. With this implicit algorithm, calculations on a resistive time scale become feasible and are being performed in the study of Reversed Field Pinches.

APPENDIX

Numerical Stability Criterion

Linearizing Eqs. (2)–(6) and Fourier analyzing, we obtain for the perturbed quantities

$$\frac{\partial \mathbf{u}}{\partial t} = (i\mathbf{k} \cdot \mathbf{B}_0)\,\mathbf{b} - i\mathbf{k}\Pi, \tag{A.1}$$

$$\frac{\partial \mathbf{b}}{\partial t} = (i\mathbf{k} \cdot \mathbf{B}_0)\,\mathbf{u} - (i\mathbf{k} \cdot \mathbf{u})\,\mathbf{B}_0, \tag{A.2}$$

$$\frac{\partial \Pi}{\partial t} = -(\Gamma p_0 + B_0^2)(i\mathbf{k} \cdot \mathbf{u}) + (i\mathbf{k} \cdot \mathbf{B}_0)(\mathbf{u} \cdot \mathbf{B}_0), \tag{A.3}$$

where $\mathbf{k}$ is the wave vector, and $\Pi = p + \mathbf{B}_0 \cdot \mathbf{b}$.

Concentrating on the compressional branch by letting $k_{||} = 0$ and applying the explicit predictor–corrector scheme, we obtain for the vector $(\mathbf{u}, \Pi)^t$ the amplification matrix

$$\mathbf{G} = \begin{pmatrix} 1 - \delta t^2 k_\perp^2 v_s^2, & -\delta t\, i k_\perp \\ -\delta t\, i k_\perp v_s^2, & 1 - \delta t^2 k_\perp^2 v_s^2 \end{pmatrix} \tag{A.4}$$

where $v_s^2 = (\Gamma p_0 + B_0^2)$ is the magnetosonic speed.

The stability criterion

$$\delta t_{\exp} |k_\perp B_0|_{\max} < 1 \tag{A.5}$$

follows from the eigenvalues of $\mathbf{G}$, where we used $p_0 \ll B_0^2$.

In contrast, the eigenvalues of the amplification matrix for the implicit equations

$$\mathbf{u}^{n+1} = \mathbf{u}^n - \delta t\, i\mathbf{k}_\perp \Pi^{n+1}, \tag{A.6}$$

$$\Pi^{n+1} = \Pi^n - \delta t\, i v_s^2 \mathbf{k}_\perp \cdot \mathbf{u}^{n+1} \tag{A.7}$$

have the magnitude

$$|\lambda| = \frac{1}{[1 + \delta t^2 k_\perp^2 v_s^2]^{1/2}} \tag{A.8}$$

implying unconditional stability. In this case, the shear Alfvén branch with $k_\perp = 0$ determines numerical stability. Letting $k_\perp = 0$ in Eqs. (A.1)–(A.3), we obtain

$$\begin{pmatrix} \mathbf{u}^{n+1} \\ \mathbf{b}^{n+1} \end{pmatrix} = \begin{pmatrix} 1 - \delta t^2 k_{||}^2 B_0^2, & i\,\delta t\, k_{||} B_0 \\ i\,\delta t\, k_{||} B_0, & 1 - \delta t^2 k_{||}^2 B_0^2 \end{pmatrix} \begin{pmatrix} \mathbf{u}^n \\ \mathbf{b}^n \end{pmatrix} \tag{A.9}$$

with the stability criterion

$$\delta t_{\text{imp}} |k_{||} B_0|_{\max} < 1, \tag{A.10}$$

which is also the stability criterion for the incompressible equations with the same predictor–corrector scheme. Since $k_{||\max} \sim M$, and $k_{\perp\max} \sim M/\delta r$, where M is the largest poloidal mode number included in the calculations

$$\frac{\delta t_{\text{imp}}}{\delta t_{\exp}} \sim \frac{k_{\perp\max}}{k_{||\max}} \sim \frac{1}{\delta r} \gg 1.$$

Note that in Eq. (A.8), $\lambda \ll 1$ for large δt, leading to damping of the compressional modes, as expected.

ACKNOWLEDGMENTS

This work was supported by Department of Energy Contract DE-FG05-80ET-53088 and NSF Contract ATM-82-14730.

REFERENCES

1. H. R. STRAUSS, *Phys. Fluids* **19** (1976), 134.
2. H. R. STRAUSS, *Phys. Fluids* **20** (1977), 1354.
3. W. PARK, D. A. MONTICELLO, AND R. B. WHITE, *Bull. Amer. Phys. Soc.* **22** (1978), 779.
4. H. R. STRAUSS, W. PARK, D. A. MONTICELLO, R. B. WHITE, S. C. JARDIN, M. S. CHANCE, A. M. TODD, AND A. M. GLASSER, *Nucl. Fusion* **5** (1980), 638.
5. W. PARK, D. A. MONTICELLO, R. B. WHITE, AND S. C. JARDIN, *Nucl. Fusion* **20** (1980), 1181.
6. H. R. HICKS, B. CARRERAS, J. A. HOLMES, D. K. LEE, AND B. W. WADDELL, *J. Comput. Phys.* **44** (1981), 46.
7. H. R. STRAUSS, *Nucl. Fusion* **23** (1983), 649.
8. R. IZZO, D. A. MONTICELLO, W. PARK, J. MANICKAM, H. R. STRAUSS, R. GRIMM, AND K. MCGUIRE, *Phys. Fluids* **26** (1983), 2240.
9. D. D. SCHNACK, D. C. BAXTER, AND E. J. CARAMANA, A pseudospectral algorithm for three-dimensional magnetohydrodynamic simulation, *J. Comput. Phys.* (1984), in press.
10. C. H. FINAN, "The Alternating-Direction Implicit Numerical Solution of the Time-Dependent, Three-Dimensional, Single Fluid, Resistive Magnetohydrodynamic Equations," Ph.D. thesis, University of California, Davis; Livermore Report UCRL-53086, 1980.
11. A. Y. AYDEMİR AND D. C. BARNES, "Proceedings of the U.S.–Japan Theory Workshop on 3D MHD Studies for Toroidal Devices, Oak Ridge, Tenn., 1981," CONF-8110101, p. 187.
12. A. Y. AYDEMIR AND D. C. BARNES, *J. Comput. Phys.* **53** (1984), 100.
13. A. Y. AYDEMIR AND D. C. BARNES, *Phys. Rev. Lett.* **52** (1984), 930.
14. A. Y. AYDEMIR AND D. C. BARNES, *Bull. Amer. Phys. Soc.* **28** (1983), 1108.
15. S. C. JARDIN, J. L. JOHNSON, J. M. GREENE, AND R. C. GRIMM, *J. Comput. Phys.* **29** (1978), 101.
16. D. GOTTLIEB AND S. A. ORSZAG, "Numerical Analysis of Spectral Methods: Theory and Application," SIAM, Philadelphia, 1977.
17. O. BUNEMAN, "VCFT, LIBRIS Abstracts (m12)," National Magnetic Fusion Energy Computer Center, Livermore, Calif.
18. R. D. RICHTMYER AND K. W. MORTON, "Difference Methods for Initial Value Problems," 2nd ed., Interscience, New York, 1967.